1362–1374 *Nucleic Acids Research, 2018, Vol. 46, No. 3* *Published online 18 December 2017*
doi: 10.1093/nar/gkx1256

Accuracy of genetic code translation and its orthogonal corruption by aminoglycosides and Mg^{2+} ions

Jingji Zhang, Michael Y. Pavlov and Måns Ehrenberg*

Department of Cell and Molecular Biology, Uppsala University, Husargatan 3, Box 596, Uppsala 75124, Sweden

Received August 06, 2017; Revised December 04, 2017; Editorial Decision December 04, 2017; Accepted December 13, 2017

ABSTRACT

We studied the effects of aminoglycosides and changing Mg^{2+} ion concentration on the accuracy of initial codon selection by aminoacyl-tRNA in ternary complex with elongation factor Tu and GTP (T_3) on mRNA programmed ribosomes. Aminoglycosides decrease the accuracy by changing the equilibrium constants of 'monitoring bases' A1492, A1493 and G530 in 16S rRNA in favor of their 'activated' state by large, aminoglycoside-specific factors, which are the same for cognate and near-cognate codons. Increasing Mg^{2+} concentration decreases the accuracy by slowing dissociation of T_3 from its initial codon- and aminoglycoside-independent binding state on the ribosome. The distinct accuracy-corrupting mechanisms for aminoglycosides and Mg^{2+} ions prompted us to re-interpret previous biochemical experiments and functional implications of existing high resolution ribosome structures. We estimate the upper thermodynamic limit to the accuracy, the 'intrinsic selectivity' of the ribosome. We conclude that aminoglycosides do not alter the intrinsic selectivity but reduce the *fraction* of it that is expressed as the accuracy of initial selection. We suggest that induced fit increases the accuracy and speed of codon reading at unaltered intrinsic selectivity of the ribosome.

INTRODUCTION

Intracellular protein synthesis relies on ribosomal translation of messenger RNA (mRNA) encoded genetic information to sequences of amino acid (aa) residues (1–4). For maximal fitness, the bacterial ribosome is composed of few large RNA chains and a large number of ribosomal proteins of small and uniform size (5) and it translates mRNA with high speed and accuracy (2,6–9). The elongation factor GTPases Tu (EF-Tu) and G (EF-G) increase the rates of binding of aminoacyl-tRNA to the ribosomal A site and translocation of mRNA and tRNAs along the ribosomal frame by five (9,10) and four (11) orders of magnitude, respectively.

Aminoacyl-tRNA (aa-tRNA) in ternary complex with EF-Tu and GTP (T_3) binds to the ribosomal A/T site (1,2). In response to matching or non-matching mRNA codon in the A site, the T_3-bound GTP is rapidly hydrolyzed allowing aa-tRNA to accommodate into the A/A site or, alternatively, intact T_3 in the GTP form rapidly leaves the ribosome (1). Initial codon selection by T_3 ends upon GTP hydrolysis (12). The accuracy of initial selection is provided by codon-anticodon interactions and amplified by activation of the monitoring bases A1492, A1493 and G530 of 16S ribosomal RNA (rRNA) for binding to the codon-anticodon helix (1,13,14). The accuracy of bacterial mRNA translation into peptide sequence is further amplified by proofreading (15–18), which occurs after hydrolysis of GTP in T_3 and leads to high-probability-dissociation of near-cognate aa-tRNA (10,19,20). Together, initial selection and proofreading ensure a remarkably high accuracy of genetic code translation *in vivo* (21,22), but there are also notably high error 'hot spots', often involving U:G mismatches (9,21,22).

Ribosome speed (11) and translation errors (7,9,12,23) are sensitive to the concentration, $[Mg^{2+}]$, of free Mg^{2+} ions. Increasing $[Mg^{2+}]$ is deleterious. It reduces the accuracy of codon reading by an incoming aa-tRNA in both initial and proofreading codon selection steps (9,10,12,24), transforms near-cognate ternary complex into competitive inhibitors of cognate codon reading (8,25) and inhibits the EF-G dependent translocation (11,26). At the same time, Mg^{2+} ions are essential for the stability of the 70S ribosome structure (27), suggesting that the intracellular Mg^{2+} concentration is fine tuned for high viability and rapid growth of bacteria (27,28). Free $[Mg^{2+}]$ in *E. coli* has been estimated to be in the 1–2 mM range (29), slightly below the $[Mg^{2+}]$ value of 2.3 mM which, together with polyamines and other components of the 'polymix' buffer (23), calibrates the accuracy of translation in the test-tube (28) to that in the bacterial cell (22).

Aminoglycosides corrupt the accuracy of initial codon selection and proofreading in genetic code translation (30–32) and inhibit EF-G dependent translocation of mRNA and tRNAs (26,33,34). They induce hyper-activation of the

*To whom correspondence should be addressed. Tel: +46 18 471 4213; Fax: +46 18 472 4262; Email: ehrenberg@xray.bmc.uu.se

monitoring bases A1492, A1493 and G530 of 16S rRNA (14,35–37) for contact not only with cognate (13,14) but also with near-cognate codon-anticodon helices in the decoding center of the ribosome (14). It has been suggested that increasing [Mg^{2+}] induces hyper-activation of the monitoring bases, thereby corrupting the accuracy of codon selection and inhibiting translocation by a similar mechanism (7,11,14). It has also been proposed that the accuracy of initial codon selection is greatly enhanced by a particular induced fit mechanism (38–40) conferring a much smaller rate constant for GTPase activation on EF-Tu in near-cognate than cognate cases (24,40,41) and, furthermore, that aminoglycosides increase the near-cognate GTPase rate constant and leaves the cognate one unaltered (30,32).

Here, we used a cell free system for ribosomal protein synthesis with *E. coli* components (12) to quantify the effects of [Mg^{2+}] and aminoglycosides on the accuracy of initial codon selection. We also measured a mean dissociation time of an A-site bound T_3, assembled with Phe-$tRNA^{Phe}$ and a GTPase deficient His84Ala EF-Tu mutant (42). The experiments were performed in absence of aminoglycosides or presence of paromomycin, gentamicin or neomycin. In contrast to earlier proposals (7,14), including our own (11), we found that high [Mg^{2+}] and aminoglycosides corrupt the accuracy of initial codon selection by different mechanisms. Both agents affect T_3-bound ribosomal complexes in a codon-anticodon independent manner but, while increasing [Mg^{2+}] selectively stabilizes the initial T_3•ribosome complex, aminoglycosides selectively stabilize the pre-GTPase T_3•ribosome complex with activated monitoring bases. We use our data to estimate the upper thermodynamic limit to the accuracy, the 'intrinsic selectivity' of the ribosome. Aminoglycosides and [Mg^{2+}] do not affect the intrinsic selectivity but, instead, decrease the fraction of it that is expressed as current accuracy. We also conclude that although an induced fit mechanism leaves the intrinsic selectivity unaltered, it may enhance both the accuracy and speed of initial codon selection on the ribosome.

MATERIALS AND METHODS

Reagents and buffer conditions

Purified *Escherichia coli* components including initiation factors, elongation factors, 70S ribosomes (MRE 600) and f[^{3}H]Met-$tRNA^{fMet}$ as well as synthetic mRNAs were prepared as described previously (9) and references therein. Native $tRNA^{Phe}$ were from Chemical Block. [^{3}H]Met and [^{3}H]GTP were from Perkin Elmer. Other chemicals were either from Sigma-Aldrich or Merck. All experiments were performed at 37°C in polymix buffer (23) containing 95 mM KCl, 5 mM NH_4Cl, 0.5 mM $CaCl_2$, 8 mM putrescine, 1 mM spermidine, 5 mM potassium phosphate, 1 mM DTE and 5 mM $Mg(OAc)_2$. The buffer also contained 1 mM ATP + 1 mM GTP for the ribosome mixture or 2 mM ATP for the ternary complex mixture and energy regenerating components: 10 mM phosphoenolpyruvate (PEP), 50 μg/ml pyruvate kinase (PK), and 2 μg/ml myokinase (MK). Extra $Mg(OAc)_2$ was added to adjust the free Mg^{2+} concentration in the reaction. Free [Mg^{2+}]varies from 1.3 to 25 mM with addition of 0 to 30 mM extra $Mg(OAc)_2$ assuming that one ATP or GTP molecule chelates one Mg^{2+} and PEP chelates Mg^{2+} with a K_d-value of 6 mM (43).

Measurement of k_{cat}/K_m for cognate initial selection reaction

Ribosome mixture contained 70S ribosomes (0.3–2 μM), f[^{3}H]Met-$tRNA^{fMet}$ (0.45–2.5 μM), mRNA (0.45–2.5 μM), IF1 (0.45–2.5 μM), IF2 (0.15–0.5 μM), IF3 (0.45–1.5 μM) in polymix buffer with the energy regeneration components and varying concentrations of extra $Mg(OAc)_2$. Ternary complex mixture contained tRNAs (2–5 μM), EF-Tu (0.15–1 μM), [^{3}H]GTP (0.15–0.5 μM), amino acid (0.2 mM) and aa-tRNA synthetase (1.5 units/μl) in polymix buffer with energy regeneration components and varying concentrations of extra $Mg(OAc)_2$. When studying the effects of aminoglycosides, 10 μM of paromomycin, gentamicin or neomycin were added to the both mixes. All the concentrations here refer to the component concentrations in the final reaction mixture.

Pre-initiated 70S ribosomes, with f[^{3}H]Met-$tRNA^{fMet}$ in the P site, were formed by incubation of the ribosome mixture at 37°C for 10 min. Ternary complexes were formed by incubating the ternary complex mixture at 37°C for 15 min. Ribosome and ternary complex mixtures were rapidly mixed in a quench-flow instrument (RQF-3, KinTek Corp.) and quenched with 17% formic acid (final concentration) at specific time points. In order to estimate the concentration of active 70S initial complexes, equal volumes (10 μl) of ribosome and ternary mixtures were also mixed with addition of EF-Ts (1.5 μM). The reaction was incubated at 37°C for 1 min followed by quenching with formic acid (17% final). All samples were centrifuged at 20 000 × g for 15 min at 4°C, and the fractions of [^{3}H]GTP and [^{3}H]GDP, or the extent of [^{3}H]dipeptide formed for the control experiments, were quantified using ion-exchange or reversed phase HPLC equipped with a β-RAM model 3 radioactivity detector (IN/US Systems) as described previously (9).

Measurement of k_{cat}/K_m for near-cognate initial selection

Near-cognate reactions were performed identically to the cognate reactions except that, in cases where near-cognate GTP hydrolysis reactions were slow, the mixing was performed manually rather than in a quench flow instrument. Transformation of [^{3}H]GDP to [^{3}H]GTP by the energy regeneration system was limited by the slow dissociation rate of GDP from EF-Tu, k_{ex_GDP}, (~0.01 s^{-1} in absence of EF-Ts). Furthermore, the slow rate of exchange of [^{3}H]GTP for unlabeled GTP on the ternary complex (k_{ex_GTP}) decreased the [^{3}H]GDP signal. For precise parameter estimation a cognate reaction was always performed in parallel with the near-cognate one (12). Two ribosome mixtures, containing mRNAs with either cognate or near-cognate A-site codon, were prepared as described above. A ternary complex mixture was also prepared as described above, and divided into two mixtures for cognate and near-cognate reaction. Ribosome and ternary complex mixtures were mixed and quenched by 17% (final) formic acid after varying incubation times. The two resulting curves (Figure 1, black and red curves), sharing the plateau of GTP hydrolysis, k_{ex_GDP}, and k_{ex_GTP}, were jointly fitted (12) (see also SI, Eq. S46

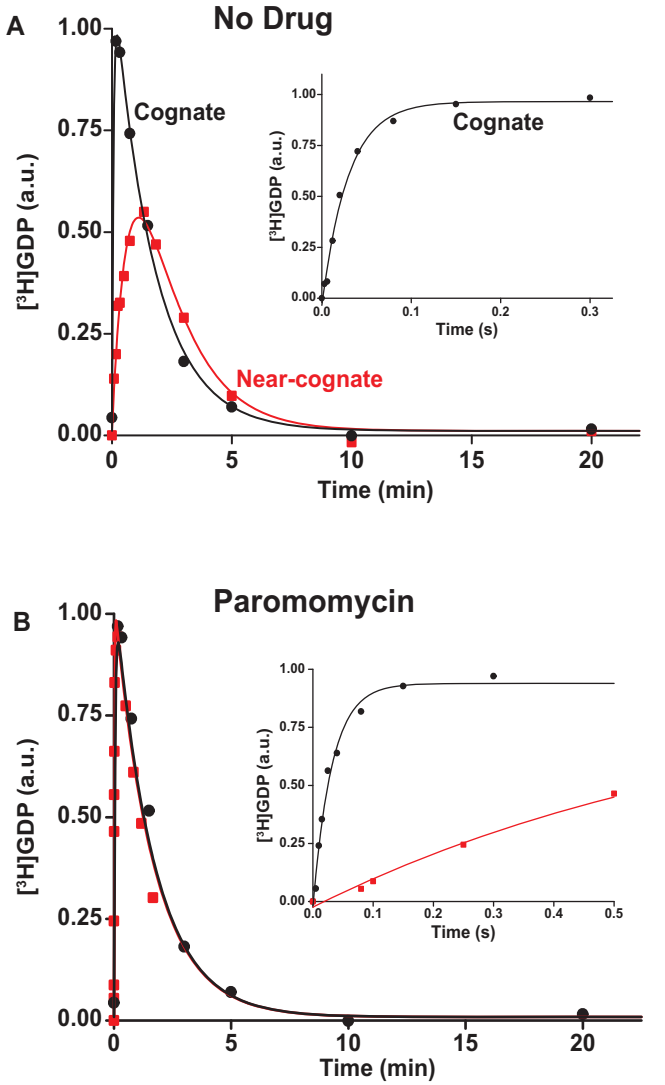

Figure 1. Effects of paromomycin on the kinetics of GTP hydrolysis on ternary complexes reading cognate (UUC) and near-cognate (CUC) codons. Time courses of [^{3}H]GDP accumulation after mixing ternary complexes [^{3}H]GTP·EF-Tu·Phe-tRNA^{Phe} with excess of mRNA programmed 70S ribosomes with cognate codon UUC (black squares) or near-cognate codon CUC (red circles) in the A-site. Cognate and near-cognate reactions were conducted in parallel at 1.3 mM free Mg^{2+} concentration (high accuracy condition). [^{3}H]GDP accumulation in fast time scale is shown in inserts. Actual rates, k, of GTP hydrolysis for T_3 reading UUC and CUC codons were obtained from fits of the corresponding curves (see M&M for details). Panel A: (no drug) $k = 34\ s^{-1}$ for UUC and $k = 0.024\ s^{-1}$ for CUC reading. Panel B: (with Paromomycin) $k = 32\ s^{-1}$ for UUC and $k = 1.3\ s^{-1}$ for CUC reading.

for details). To estimate active ribosome concentration for near-cognate reactions, a separate ternary complex mixture was prepared with the corresponding cognate tRNA in the presence of EF-Ts (1.5 μM), and reacted with the ribosome complex in equal volumes (10 μl). Analysis of all ^{3}H-labeled products was performed as described for the cognate reactions.

Chase of $T_{3(H84A)}$ by wild type T_3

A GTPase deficient EF-Tu mutant (H84A) (42) was used to prepare a a ternary complex, $T_{3(H84A)}$, mixture as described above in the section 'Measurement of k_{cat}/K_m for cognate initial selection reaction'. $T_{3(H84A)}$ was pre-bound to mRNA programmed ribosomes with a cognate codon in the A site in the absence of drug or presence of 10 μM Par, Gen or Neo. The mean dissociation time, τ_{diss1} of $T_{3(H84A)}$ was estimated in chase experiments by addition of native cognate T_3 with wild type EF-Tu in a five-fold smaller concentration than $T_{3(H84A)}$ in the absence and in equal concentration in the presence of drugs. The time course of dipeptide formation was then measured essentially as described above in the section 'Measurement of k_{cat}/K_m for cognate initial selection reaction' except that the mixing was done manually. The experiments were performed at 2.3 mM free [Mg^{2+}], a concentration at which the accuracy of our cell-free protein synthesis system matches that in the living *E. coli* cell (22,28). To obtain the mean dissociation time, τ_{diss1}, of $T_{3(H84A)}$, the mean time of dipeptide formation was multiplied by a factor of six in the absence and by a factor of two in the presence of aminoglycosides. The rationale behind such a correction is that at the native T_3 concentration 5-fold below that of $T_{3(H84A)}$ the probability of native T_3 binding after $T_{3(H84A)}$ dissociation and, hence, of dipeptide formation is only one per six. This effectively slows dipeptide formation rate in the absence of drug by a factor of six making it possible to conduct the experiment 'by hand'. At equal T_3 and $T_{3(H84A)}$ concentrations the probability of native T_3 binding after $T_{3(H84A)}$ dissociation is one per two and the dipeptide formation rate is slowed by the same factor. Details of this procedure are provided in SI (see Eq. S33).

RESULTS

Accuracy of initial codon selection and its tuning by Mg^{2+} ions and aminoglycosides

We studied the effects of varying free [Mg^{2+}] in the 1.3–25 mM interval and aminoglycoside addition on the kinetic efficiency, $(k_{cat}/K_m)_I^x$, of cognate ($x = c$) UUC (Phe) or near-cognate ($x = nc1$) CUC (Leu), (x = *nc2*) UCC (Ser) or (x = *nc3*) UUA (Leu) codon reading by Phe-tRNA^{Phe} in ternary complex (T_3) with EF-Tu and GTP. The experiments were performed in the absence of aminoglycoside ($I = 0$) or in the presence of paromomycin ($I = P$), gentamicin ($I = G$) or neomycin ($I = N$). A single T_3 solution was prepared for mixing with each one of solutions containing mRNA programmed ribosomes with fMet-tRNA^{fMet} in the P site and a UUC, CUC, UCC or UUA codon in the A site (see Materials and Methods). GTP hydrolysis reactions were started by mixing equal volumes of T_3 and ribosome solutions. The reactions were quenched by formic acid at different incubation times and the extent of GTP hydrolysis was quantified as described in Materials and Methods. The mRNA programmed 70S ribosomes were always present in excess over T_3, and the rate of GTP hydrolysis (k), defined as the inverse of the mean time for the hydrolytic reaction (44), was measured at several concentrations, [R_1], of active ribosomes. Conditional on proportionality between k and [R_1], (k_{cat}/K_m)-values were estimated as $k/[R_1]$ (12). In

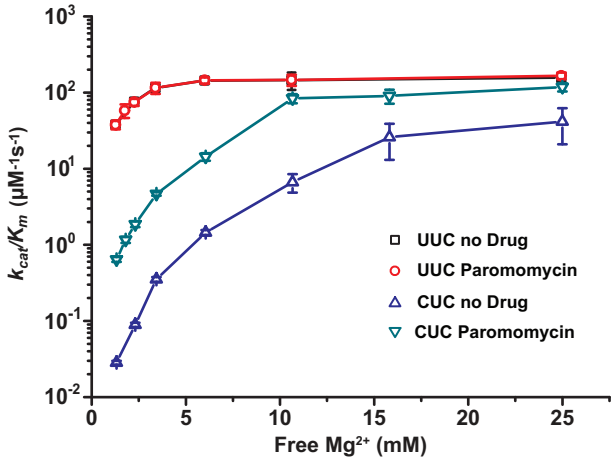

Figure 2. Effects of [Mg^{2+}] and paromomycin on the kinetic efficiency (k_{cat}/K_m) of cognate and near-cognate GTPase reactions. Log_{10}-values of k_{cat}/K_m of GTP hydrolysis in T_3 ([^{3}H]GTP·EF-Tu·Phe-tRNA^{Phe}) reading cognate (UUC) or near-cognate (CUC) codonplotted as functions of [Mg^{2+}] in the presence (○, UUC; ▽, CUC) or absence (□, UUC; △, CUC) of paromomycin.

cognate cases, hydrolysis of [^{3}H]GTP was much faster than regeneration of [^{3}H]GTP from EF-Tu bound [^{3}H]GDP, allowing for estimation of the k parameter directly from single exponential fitting (Figure 1A, insert). In near-cognate cases, GTP hydrolysis reaction was much slower (Figure 1A). Therefore estimation of k required concomitant determination of the rate of [^{3}H]GTP regeneration from EF-Tu bound [^{3}H]GDP and the rate of exchange of [^{3}H]GTP in T_3 with unlabeled, free GTP (see Materials and Methods for details). The addition of paromomycin had negligible effect on the rate, k, of GTP hydrolysis reaction in the cognate cases (Figure 1B, insert) but increased greatly the k-values of the near-cognate reactions (Figure 1B and B insert). Also gentamicin and neomycin addition had negligible effect on the cognate k-value but increased the rate of near-cognate GTP hydrolysis reaction by even larger factors than paromomycin (see Supplementary Figure S1).

Estimates of cognate $(k_{cat}/K_m)_0^c$ and $(k_{cat}/K_m)_P^c$ as well as near-cognate $(k_{cat}/K_m)_0^{nc1}$ and $(k_{cat}/K_m)_P^{nc1}$ parameters at different [Mg^{2+}] values are plotted in Figure 2. The [Mg^{2+}] dependencies of cognate $(k_{cat}/K_m)_I^c$ parameters and near-cognate $(k_{cat}/K_m)_I^{nci}$ parameters for reading the CUC, UCC and UUA near-cognate codons in the absence of aminoglycosides and in the presence of paromomycin, gentamicin or neomycin are shown in Supplementary Figures S2 and S3. In the cognate cases, the [Mg^{2+}] dependent parameters $(k_{cat}/K_m)_0^c$ and $(k_{cat}/K_m)_P^c$ are virtually identical (Figure 2) as they increase from 37 $\mu M^{-1}s^{-1}$ at 1.3 mM free [Mg^{2+}] to a plateau value of 150 $\mu M^{-1}s^{-1}$ at 25 mM [Mg^{2+}]. At the same time, the [Mg^{2+}] dependencies of near–cognate $(k_{cat}/K_m)_0^{nc1}$ and $(k_{cat}/K_m)_P^{nc1}$ differ greatly (Figure 2). At 1.3 mM [Mg^{2+}], $(k_{cat}/K_m)_0^{nc1}$ is more than three orders of magnitude smaller than $(k_{cat}/K_m)_0^c$ while $(k_{cat}/K_m)_P^{nc1}$ is about 20-fold larger than $(k_{cat}/K_m)_0^{nc1}$. At increasing [Mg^{2+}] all curves in Figure 2 converge towards similar plateau values. The cognate $(k_{cat}/K_m)_I^c$ values are very similar for $I = 0$, P, G and N and inequalities $(k_{cat}/K_m)_0^{nci} < (k_{cat}/K_m)_P^{nci} < (k_{cat}/K_m)_G^{nci} < (k_{cat}/K_m)_N^{nci}$ hold for all studied near-cognate codons (CUC ($i = 1$), UCC ($i = 2$) and UUA ($i = 3$)) at all values of [Mg^{2+}] (Figure 2, Supplementary Figures S2 and S3). From these data we infer that the error induction mechanisms of Mg^{2+} ions and aminoglycosides are distinct (see Discussion).

Impact of aminoglycosides on efficiency-accuracy trade-off in initial codon selection

Using data presented in the previous section the cognate codon reading efficiency, $(k_{cat}/K_m)_I^c$, was plotted versus the initial codon selection accuracy, $A_I^{nci} = (k_{cat}/K_m)_I^c/(k_{cat}/K_m)_I^{nci}$ in the absence ($I = 0$) or presence of different aminoglycosides (I = P, G or N) and near-cognate codons CUC ($i = 1$), UCC ($i = 2$) or UUA ($i = 3$) at varying [Mg^{2+}] (Figure 3). Linear efficiency-accuracy trade-off plots (9,12) were obtained in all cases as shown for $i = 1$, 2 or 3 in Figure 3A, B or C, respectively. All trade-off lines are accounted for by Equation (1) (derived in SI, Eq. S14) with [Mg^{2+}]-independent k_1 and d_{eI}^{nci} parameters (12):

$$\left(\frac{k_{cat}}{K_M}\right)_I^c = k_1 \frac{d_{eI}^{nci} - A_I^{nci}}{d_{eI}^{nci} - 1}, \qquad (1)$$

The rate constant for association of ternary complex to the ribosome, k_1, is estimated as the value of $(k_{cat}/K_M)^c$ at the intercept of a trade-off line with the vertical $A = 1$ axis. The effective selectivity parameter, d_{eI}^{nci}, is operationally defined from the A-value of the intercept of each trade-off line with the horizontal $(k_{cat}/K_M)^c = 0$ axis (Figure 3). From the plots in Figure 3 k_1 was estimated as 150 $\mu M^{-1}s^{-1}$ and the d_{eI}^{nci} values in the absence of drugs as $d_{e0}^{nc1} = 1760$, $d_{e0}^{nc2} = 5900$ and $d_{e0}^{nc3} = 1200$. The latter estimates are very similar to those obtained in previous work for the same tRNA and near-cognate codons (9). The d_{e0}^{nci}-value decreased to $d_{eP}^{nc1} = 75$, $d_{eP}^{nc2} = 420$ and $d_{eP}^{nc3} = 110$ by addition of paromomycin; to $d_{eG}^{nc1} = 17$, $d_{eG}^{nc2} = 100$ and $d_{eG}^{nc3} = 15$ by addition of gentamicin; and to $d_{eN}^{nc1} = 3.9$, $d_{eN}^{nc2} = 30$ and $d_{eN}^{nc3} = 9$ by addition of neomycin (Table 1). The fold decrease in d_{e0}^{nci} upon aminoglycoside addition was in each case quantified as a $d_{e0}^{nci}/d_{eI}^{nci}$ ratio, as shown for $i = 1$, 2, 3 and I = P, G, N in Table 1. Importantly, the $d_{e0}^{nci}/d_{eI}^{nci}$ ratios in Table 1 also quantify the fold of aminoglycoside-induced decrease in current accuracy of initial codon selection (A_0^{nci}/A_I^{nci}) at any Mg^{2+} ion concentration. This follows from linearity of the trade-off plots in Figure 3 and from the aminoglycoside-insensitivity of the cognate $(k_{cat}/K_m)_I^c$ parameters (Figure 2 and Supplementary Figure S2). Therefore, these ratios also estimate the effects of aminoglycosides on the initial selection accuracy in the living cell. The $d_{e0}^{nci}/d_{eI}^{nci}$ ratios are similar for different near-cognate codons (different i-values). We defined average ratios, $d_{e0}^{nc}/d_{eI}^{nc} = (1/3)\sum_{i=1}^{3} d_{e0}^{nci}/d_{eI}^{nci}$, to estimate the decrease in effective selectivity of codon reading by paromomycin ($d_{e0}^{nc}/d_{eP}^{nc} = 16$), gentamicin ($d_{e0}^{nc}/d_{eG}^{nc} = 80$) and neomycin ($d_{e0}^{nc}/d_{eN}^{nc} = 260$) (Table 2). Although neomycin and paromomycin induce

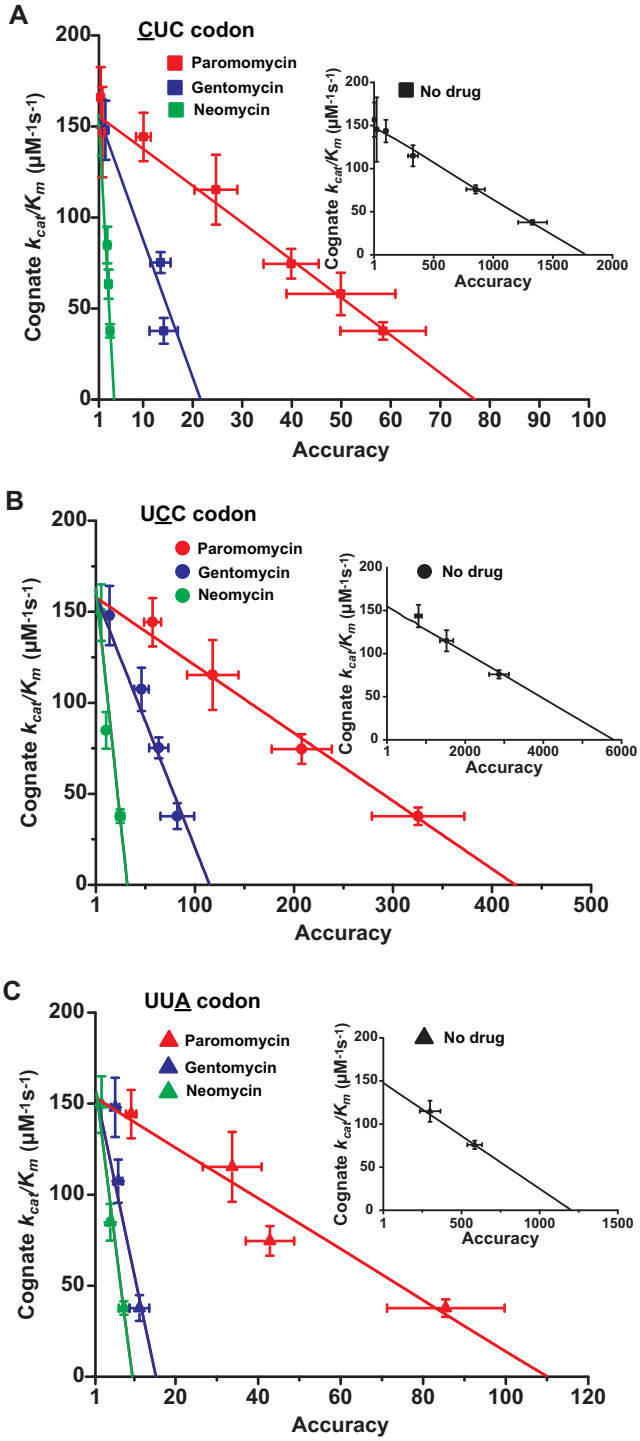

Figure 3. The effect of aminoglycosides on the efficiency-accuracy trade-off. Kinetic efficiency $(k_{cat}/K_m)^c$ of the reaction of GTP hydrolysis on EF-Tu·GTP·Phe-tRNA^{Phe} ternary complex reading its cognate UUC codon was plotted versus accuracy of initial selection for the same ternary complex reading its near-cognate codons in the presence of paromomycin, gentamicin and neomycin or in their absence (inserts). The intercepts of straight lines with the accuracy axis (*A*-value when $(k_{cat}/K_m)^c = 0$) give the effective selectivity values d_{eI}^{nci} compiled in Table 1. Panel **A**: CUC near-cognate codon; Panel **B**: UCC near-cognate codon; Panel **C**: UUA near-cognate codon.

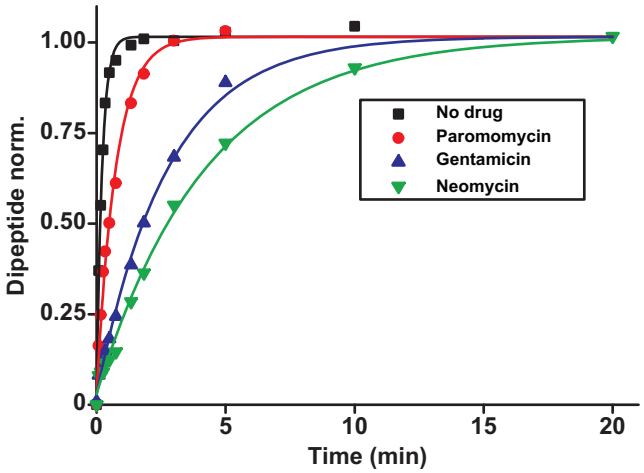

Figure 4. The effects of aminoglycosides on the dissociation-mean-time of GTPase-deficient cognate ternary complex. Time traces of dipeptide formation mirrow slow dissociation of GTPase deficient T_3 (EF-Tu(H84A)·GTP·Phe-tRNA^{Phe}), pre-bound to the A site of mRNA programmed ribosomes. The chase of GTPase deficient cognate T_3 by native cognate T_3 was conducted in the absence of aminoglycoside or in the presence of paromomycin, gentamicin or neomycin (see Materials and Methods for details).

similar structural arrangements of the decoding center (45), neomycin reduces the effective selectivity by a much larger factor than does paromomycin (Table 2).

Aminoglycoside addition reduces the rate of cognate ternary complex dissociation from the ribosome

A possible explanation for the observed aminoglycoside specific reduction of the accuracy of initial selection is a change in the equilibrium constant connecting the 'inactive conformation' of the monitoring bases with their active conformation in which they contact the codon-anticodon helix (1,2,14). These contacts are expected to stabilize cognate compared to near-cognate T_3 binding (14). To quantify the magnitude of such aminoglycoside induced stabilization of cognate T_3 binding we studied the effect of aminoglycosides on the mean-time of dissociation of a GTPase deficient ternary complex, $T_{3(H84A)}$, from mRNA programmed ribosomes with (initiator) fMet-tRNA^{fMet} in P site and cognate UUC (Phe) codon in A site. This ternary complex contained Phe-tRNA^{Phe}, the GTPase deficient EF-Tu mutant, H84A, (42) and GTP. $T_{3(H84A)}$ was pre-bound to the ribosome and then chased from it by addition of GTPase proficient T_3 assembled with native EF-Tu and GTP. The mean time for $T_{3(H84A)}$ dissociation, $\tau_{diss\,I}$, was estimated from the mean time of fMet-Phe-tRNA^{Phe} dipeptide formation (Figure 4) as described in Materials and Methods. Estimates of $\tau_{diss\,I}$ obtained in the absence of aminoglycoside ($I = 0$) or in the presence of paromomycin ($I = P$), gentamicin ($I = G$) or neomycin ($I = N$) are summarized in Table 1 and presented as ratios $\tau_{diss\,I}/\tau_{diss0}$ for $I = P$, G and N in Table 2. It is seen that ratios $\tau_{diss\,I}/\tau_{diss0}$ are very similar to ratios d_{e0}^{nc}/d_{eI}^{nc} for $I = P$, G and N (Table 2). From the close similarity of these ratios we propose that the origin of error induction by aminoglycosides is, indeed, a shift of equilibrium of the monitor-

Table 1. Dissociation time, $\tau_{diss\,I}$, of the GTPase deficient cognate ternary complex and effective selectivity, d_{eI}^{nci}, for different near-cognate codons with and without drugs

	No drug	Paromomycin	Gentamicin	Neomycin
Dissociation time, $\tau_{diss\,I}$(s)	2 ± 0.1	26 ± 1	130 ± 4	320 ± 15
Fold increase by drug		13 ± 1	65 ± 4	160 ± 11
d_{eI}^{nc1}-value on C̲UC	1760 ± 180	75 ± 10	17 ± 4	3.9 ± 0.6
Fold decrease by drug		23 ± 4	104 ± 27	451 ± 84
d_{eI}^{nc2}-value on UC̲C	5900 ± 970	420 ± 76	103 ± 20	30 ± 5
Fold decrease by drug		14 ± 4	57 ± 15	197 ± 46
d_{eI}^{nc3}-value on UUA̲	1200 ± 190	111 ± 22	14.6 ± 0.8	9 ± 1.7
Fold decrease by drug		11 ± 3	82 ± 14	133 ± 33

Table 2. Average fold decrease, d_{e0}^{nc}/d_{eI}^{nc}, in effective selectivity compared with fold increase in dissociation time, $\tau_{diss\,I}/\tau_{diss0}$, of the GTPase deficient cognate T_3 upon aminoglycoside addition

	d_{e0}^{nc}/d_{eI}^{nc}	$\tau_{diss\,I}/\tau_{diss0}$
No drug	1	1
Paromomycin	16 ± 2	13 ± 1
Gentamicin	81 ± 12	65 ± 4
Neomycin	260 ± 34	160 ± 11

ing bases from their inactive to their active states, and that the underlying relative change in equilibrium constant is the same for cognate and near-cognate codon–anticodon interactions, as explained in detail in Discussion.

DISCUSSION

Key observations of the present work

- The kinetic efficiency, k_{cat}/K_m, of the cognate GTP hydrolysis reaction is unaffected by aminoglycosides but increases four-fold as the free [Mg^{2+}] increases from 1.3 to 25 mM (Figure 2, Supplementary Figure S2).
- The corresponding near-cognate k_{cat}/K_m-values increase by orders of magnitude in response to aminoglycoside addition in the low Mg^{2+} concentration range and increase further with increasing [Mg^{2+}] up to the cognate k_{cat}/K_m-values (Figure 2, Supplementary Figure S3).
- The efficiency-accuracy trade-off plots (Figure 3) are linear for all near-cognate codons both in the absence and presence of the aminoglycosides (Figure 3).
- In response to aminoglycoside addition the mean dissociation time of a cognate, GTPase deficient ternary complex increase by the very same aminoglycoside specific factors (Figure 4, Table 2) as those seen for the decrease in the accuracy-axis intercepts of the efficiency-accuracy lines (Figure 3, Table 2).

To account for these key observations we have developed a kinetic model for initial codon selection by ternary complex.

Kinetic modeling of initial codon selection

Initial selection of ternary complex proceeds through sequential formation of at least three structurally distinct T_3-bound ribosome complexes (2–4,46). Therefore, realistic modeling of this kinetic process requires a scheme with at least four steps (47,48), leading from free T_3 and free ribosome (R_I) to GTP hydrolysis in complex C_4 (Figure 5). R_1 is here the mRNA-programmed ribosome with a P-site peptidyl-tRNA and an empty A site. Binding of T_3 to R_1 leads to reversible formation of the first T_3-bound complex, C_2, with association and dissociation rate constants k_1 and q_2, respectively. T_3 has the same classical, 'straight' conformation in C_2 as in its free state (49), and is unable to make codon-anticodon contact (24,47,50). Therefore rate constants k_1 and q_2 are codon unspecific and the same for cognate and near-cognate T_3. More recently, cryo electron microscopy (cryo-EM) has confirmed the lack of codon-anticodon contact in C_2 (structure I or T in the cryo-EM nomenclature) (46), and shown the decoding center of the ribosome in C_2 to be very similar to that in the mRNA-programmed ribosomes with P-site tRNA and empty A site (51). In complex C_3, emerging from C_2 with rate constant k_2, the aa-tRNA of T_3 is 'bent', allowing for proper codon-anticodon contact (52–54), and the 30S subunit has an 'open' conformation (14), like in C_2. Complex C_3 has been observed by single molecule FRET (47) and more recently by cryo-EM (structure II or A*/T in the cryo-EM nomenclature) (46). In C_3 there is codon-anticodon contact, monitoring base A1493 is more ordered than in C_2 and makes contact with the codon-anticodon helix, but otherwise the decoding centers of C_2 and C_3 are similar (46). Complex C_3 may move backward to complex C_2 or forward to complex C_4 with rate constants q_3^x or k_{3I}, respectively, where index x signifies cognate (c) or near-cognate (nc) codon-anticodon interaction and index I signifies the absence (I = 0) or presence (I = P,G or N) of drug. Rate constant q_3^x is determined by the stability of codon-anticodon interaction in the absence of monitoring base contribution. The rate constant for monitoring bases activation, k_{3I}, increases in response to aminoglycoside addition but is neutral to the cognate or near-cognate status of the codon-anticodon contact. In complex C_4, the interactions between codon-anticodon helix and monitoring bases A1492, A1493 and G530 are fully developed (13) and the 30S subunit is 'closed' (14) with monitoring bases G530 and A1492 now hydrogen-bonded (13,14). Complex C_4, in which the decoding center has similar geometry for cognate and near-cognate tRNAs, has been observed in structures of the mRNA programmed 70S ribo-

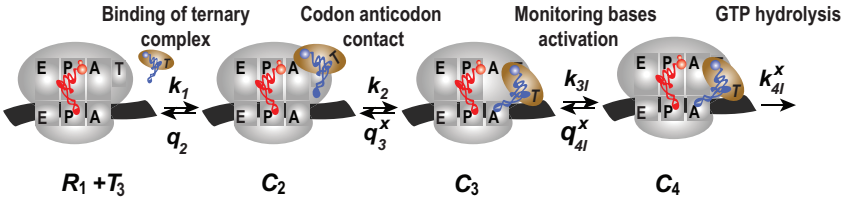

Figure 5. Four steps scheme of initial codon selection by ternary complex on mRNA programmed ribosomes. R_1 is the mRNA-programmed ribosome with empty A-site and peptidyl-tRNA in the P-site; T_3 is free ternary complex. Binding of T_3 to R_1 results in initial complex C_2 in which the anticodon of aa-tRNA in T_3 lacks contact with the mRNA codon. In complex C_3 aa-tRNA in T_3 is 'bent', its anticodon is in contact with the mRNA codon and monitoring bases A1492, A1493 and G530 are in 'inactive conformation'. In complex C_4, the monitoring bases are activated and interact with the codon-anticodon helix promoting a 'closure' of the 30S subunit (see main text for details).

some with P- and A- site tRNAs (55,56). In recent cryo-EM work (46) C_4 was visualized also for near-cognate T_3 and its striking similarity with the cognate C_4 complex, previously observed in crystallographic (54) and cryo-EM (57) studies, has been confirmed. Complex C_4 moves backward to complex C_3 with rate constant q^x_{4I} or forward to GTP hydrolysis with rate constant k^x_{4I}. The value of rate constant q^x_{4I} for monitoring bases de-activation upon their dissociation from the codon-anticodon helix and 're-opening' of the 30S subunit depends on the cognate or near-cognate status of the codon-anticodon interaction and the presence or absence of aminoglycosides. The equilibrium constants connecting ribosomal states (C_2, C_3) and (C_3, C_4) are defined as $K^x_{23} = q^x_3/k_2$ and $K^x_{34I} = q^x_{4I}/k_{3I}$, respectively. We stress here that state C_4 in Figure 5 is the last ground state on the pathway to GTP hydrolysis with activation free energy barrier$\Delta G^x_{4,\#}$. The GTP hydrolysis rate constant, k^x_{4I} is therefore given by $k^x_{4I} = \nu \cdot \exp(\Delta G^x_{4,\#}/RT)$, where ν is a frequency factor (39) and the $\Delta G^x_{4,\#}$ barrier accounts for conformational changes in EF-Tu that organize its catalytic center and the chemistry of GTP hydrolysis (42,58). Whether k^x_{4I} is neutral or sensitive to the cognate or near-cognate nature of the codon-anticodon contact and the presence or absence of aminoglycosides will be discussed below, but first we outline pertinent kinetics and accuracy characteristics of the codon recognition scheme in Figure 5.

Mg^{2+} ions and aminoglycosides have orthogonal effects on the accuracy of initial codon selection

The k_{cat}/K_m value for ribosome dependent GTP hydrolysis in a ternary complex is, firstly, determined by the rate constant, k_1, of T_3 association to the ribosome and, secondly, by the probability, p^x_I, that formation of initial complex C_2 between the ribosome and a cognate ($x = c$) or near-cognate ($x = nc$) T_3 leads to GTP hydrolysis on EF-Tu rather than dissociation of intact T_3 from the ribosome (8). The cognate $k_{\rm cat}/K_{\rm m}$-value for the kinetic scheme in Figure 5 is given by

$$\left(\frac{k_{cat}}{K_m}\right)^c_I = k_1 p^c_I = \frac{k_1}{1 + a_2(1 + a^c_{3I}(1 + a^c_{4I}))}, \qquad (2)$$

where $a_2 = q_2/k_2$, $a^c_{3I} = q^c_3/k_{3I}$ and $a^c_{4I} = q^c_{4I}/k^c_{4I}$ are discard parameters (see SI, Eq. S6, for details). Crystallographic studies have shown that aminoglycoside binding displaces the monitoring bases A1492 and A1493 from their binding sites in helix h44 of 16S rRNA greatly favoring their active, 'flipped out' conformations, in which they interact with the codon-anticodon helix (13,45,59). Aminoglycosides are, therefore, expected to increase the forward rate constant k_{3I} for monitoring bases binding to the codon-anticodon helix. By this mechanism, they decrease both the cognate discard parameter a^c_{3I} and the equilibrium constant $K^c_{34I} = q^c_{4I}/k_{3I}$ between complexes C_3 and C_4, thereby shifting their equilibrium further towards C_4. This equilibrium shift is here observed as an aminoglycoside specific increase in the mean-time of dissociation of a GTPase deficient T_3 originally in cognate complex C_4 (Figure 4 and Discussion below). We note that aminoglycoside dependent reductions in a^c_{30} do not affect the cognate $(k_{\rm cat}/K_{\rm m})^c$ parameter at any Mg^{2+} concentration (Figure 2 and Supplementary Figure S2). This implies that a^c_{30} and the product $a^c_{30}a^c_{40}$ are much smaller than one also in the absence of aminoglycosides, so that their further reduction by aminoglycosides has no effect on the cognate $k_{\rm cat}/K_{\rm m}$-value and Equation (2) is approximated by:

$$\left(\frac{k_{\rm cat}}{K_{\rm m}}\right)^c_I = k_1 p^c_I \approx \frac{k_1}{1 + a_2} \qquad (3)$$

The lack of sensitivity of the cognate $k_{\rm cat}/K_{\rm m}$ and, hence, a_2 parameter, to aminoglycosides suggests that neither q_2 nor k_2 is aminoglycoside sensitive. The increase in cognate $k_{\rm cat}/K_{\rm m}$-value with increasing [Mg^{2+}] can now be explained by a decrease in the discard parameter a_2 caused by decreasing dissociation rate constant q_2. We note that in an early study of the initial ribosome binding state for T_3, the decrease in $K_{12} = q_2/k_1$ with increasing [Mg^{2+}] was identified but originally ascribed to increasing association rate constant k_1 (60).

Near-cognate $k_{\rm cat}/K_{\rm m}$-values are given by (see SI, Eq. S6, for details):

$$\left(\frac{k_{\rm cat}}{K_{\rm m}}\right)^{nc}_I = k_1 p^{nc}_I = \frac{k_1}{1 + a_2(1 + a^{nc}_{3I}(1 + a^{nc}_{4I}))}, \qquad (4)$$

where $a^{nc}_{3I} = q^{nc}_3/k_{3I}$ and $a^{nc}_{4I} = q^{nc}_{4I}/k^{nc}_{4I}$ are near-cognate discard parameters. The current accuracy, A, of initial codon selection is defined by the ratio between cognate and near-cognate $k_{\rm cat}/K_{\rm m}$-values (39):

$$A = \frac{(k_{\rm cat}/K_{\rm m})^c}{(k_{\rm cat}/K_{\rm m})^{nc}} = \frac{1 + a_2(1 + a^{nc}_{3I}(1 + a^{nc}_{4I}))}{1 + a_2(1 + a^c_{3I}(1 + a^c_{4I}))} \qquad (5)$$

Accordingly, small a_2-value at high [Mg^{2+}] renders low accuracy of initial codon selection (8,12,24,50), and large

a_2-value at low [Mg^{2+}] renders high accuracy (12), approaching the effective initial codon selectivity, defined as A in the limit where a_2 goes to infinity in Equation (5):

$$d_{eI}^{nc} = \frac{1 + a_{3I}^{nc}(1 + a_{4I}^{nc})}{1 + a_{3I}^{c}(1 + a_{4I}^{c})} \approx a_{3I}^{nc} a_{4I}^{nc} \quad (6)$$

The effective selectivity, d_{eI}^{nc}, can be operationally defined as the A-axis intercept of a linear efficiency-accuracy plot (Figure 3) (12). Large values of d_{eI}^{nc} (Table 1) imply that the discard parameters a_{3I}^{nc} and a_{4I}^{nc} are much larger than one, allowing for the simplifying $d_{eI}^{nc} \approx a_{3I}^{nc} a_{4I}^{nc}$ approximation in Equation (6).

All efficiency-accuracy plots in the present work are linear both in the presence and absence of aminoglycosides (Figure 3), implying that neither the d_{eI}^{nc}-parameter (see Equation 1) nor the a_{3I}^{nc} and a_{4I}^{nc} parameters vary with changing [Mg^{2+}]. It has been suggested that Mg^{2+} ions and aminoglycosides affect the accuracy of initial codon selection similarly by occupying the aminoglycoside binding site in h44, thereby driving the monitoring bases to their 'flipped out', activated conformation (7,11,14). Contrary to these previous speculations, the present results mean that increasing [Mg^{2+}] does not activate A1492 and A1493, and only reduces the dissociation rate constant q_2. From this follows that Mg^{2+}- ions and aminoglycosides affect different steps of the initial selection process and thus have 'orthogonal' modes of action. This conclusion is also in line with the strikingly different effects of Mg^{2+} ions and aminoglycosides on the Michaelis-Menten rate constant, $k_{cat\,I}^{nc}$ of the GTPase reaction for near-cognate ternary complex. That is, while large [Mg^{2+}] variation had only small effect on k_{cat0}^{nc}, paromomycin addition increased k_{cat0}^{nc} by more than one order of magnitude (see Supplementary Figure S4).

Aminoglycosides do not affect the intrinsic selectivity of the ribosome

In the present context (Figure 5) the intrinsic (ultimate) selectivity of the ribosome, D_I^{nc}, is defined as:

$$D_I^{nc} = \frac{a_{3I}^{nc}}{a_{3I}^{c}} \cdot \frac{a_{4I}^{nc}}{a_{4I}^{c}} = D_{3I}^{nc} \cdot D_{4I}^{nc} \quad (7)$$

This corresponds to the current accuracy, A, in the limit where discard parameters a_{4I}^{c} and a_{4I}^{nc} in Equation (5) go to infinity at unaltered a_{4I}^{nc}/a_{4I}^{c} ratio. In this limit the concentrations of the ribosomal complexes in Figure 5 are in thermodynamic equilibrium not only in near-cognate but also in cognate cases, so that D_I^{nc} can be defined in terms of standard free energies, as in Equation (8) below. The intrinsic selectivity D_I^{nc} does not depend on discard parameter a_2 and, hence, on [Mg^{2+}]. Ratios $D_{3I}^{nc} = a_{3I}^{nc}/a_{3I}^{c}$ and $D_{4I}^{nc} = a_{4I}^{nc}/a_{4I}^{c}$ are the intrinsic selectivity arising from codon-anticodon interactions alone and the selectivity amplification by activated monitoring bases, respectively. Parameter D_{4I}^{nc}, previously ascribed to a 'geometric' selectivity amplification (13,14), has more recently been ascribed to the creation of a water free environment around the codon-anticodon helix (61). In this environment the lack of base-to-base H-bonds in near-cognate codon-anticodon helices cannot be compensated by base-to-water H-bonds, resulting in a larger standard free energy gap between a near-cognate and a cognate codon-anticodon helix than in bulk water (39,61).

Recasting Equation (7) in terms of the equilibrium and rate constants of Figure 5 leads to (see SI, Eq. S20, for details):

$$D_I^{nc} = \frac{K_{12} K_{23}^{nc} K_{34I}^{nc}}{K_{12} K_{23}^{c} K_{34I}^{c}} \frac{k_{4I}^{c}}{k_{4I}^{nc}} = \exp\left[(\Delta G_{1,\#}^{nc} - \Delta G_{1,\#}^{c})/RT\right] \quad (8)$$

It follows that D_I^{nc} is a fundamental parameter determined by the difference in standard free energy for near-cognate and cognate substrates to reach their transition states on the enzyme from their free states (39). D_I^{nc} provides, therefore, an upper, thermodynamic bound for the accuracy of initial codon selection on the ribosome.

Although aminoglycosides greatly reduce accuracy, A, and effective selectivity, d_{eI}^{nc}, of initial codon reading they leave the intrinsic selectivity, D_I^{nc}, unaltered. This inference follows from our finding that the factors $\tau_{diss\,I}/\tau_{diss0}$ by which aminoglycosides increase the mean dissociation times, $\tau_{diss\,I}$, of cognate, GTPase deficient T_3 are very similar to the factors d_{e0}^{nc}/d_{eI}^{nc} by which they decrease effective selectivity d_{eI}^{nc} (Table 2). It follows, therefore, that:

$$\frac{\tau_{diss\,I}}{\tau_{diss0}} \approx \frac{d_{e0}^{nc}}{d_{eI}^{nc}}, \quad (9)$$

for I = P, G and N (Table 2). Taking into account that $\tau_{diss\,I}$ can be approximated as (see SI, Eq. S31, for details):

$$\tau_{diss\,I} \approx \frac{1}{a_{3I}^{c} a_{4I}^{c} k_{4I}^{c}} \cdot \frac{1 + a_2}{a_2}, \quad (10)$$

one obtains from Equations (6), (7) and (9) that:

$$D_I^{nc} \approx D_0^{nc} \frac{k_{40}^{c}}{k_{4I}^{c}} \quad (11)$$

This means, in other words, that the intrinsic selectivity in the presence of aminoglycosides, $D_{I\neq0}^{nc}$, is equal to that in their absence, D_0^{nc}, multiplied by the ratio k_{40}^{c}/k_{4I}^{c} of cognate GTPase rate constants. At 37°C, the rate constant k_{40}^{c} is larger than 900 s^{-1} but a precise estimate of its value is difficult to obtain (44). In line with previous suggestions, we deem it likely that rate constant k_{40}^{c} has been maximized by optimization of the interaction between rRNA (A2662 in the sarcin-ricin loop) and the GTPase center of EF-Tu for maximal rate of GTP hydrolysis (46,54,61,62). Furthermore, structures of the mRNA programmed ribosome with cognate tRNA in the A site or of the 30S subunit with cognate ASLs have shown paromomycin to have but a marginal effect on the geometry of the decoding center and virtually no effect on the geometry of the codon-anticodon helix (13,14,55,56). To the extent that these structural features pertain also to the ternary complex in state C_4, which we deem as likely (48), they suggest that aminoglycoside addition leaves the cognate GTPase rate constant k_{40}^{c} unchanged, i.e. $k_{4I}^{c} = k_{40}^{c}$. It then follows from Equation (11) that $D_I^{nc} = D_0^{nc}$, which means that aminoglycosides greatly reduce the effective selectivity, d_{eI}^{nc}, but leave the intrinsic selectivity, D_I^{nc}, of the ribosome unaltered.

How aminoglycosides reduce the effective selectivity of initial codon reading

To see how the reduction of d_{eI}^{nc} -values by aminoglycosides (Table 2) comes about we recast Equation (6) in terms of equilibrium and rate constants (see SI, Eq. S16, for details):

$$d_{eI}^{nc} \approx a_{3I}^{nc} a_{4I}^{nc} = K_{34I}^{nc} \cdot \frac{q_3^{nc}}{k_{4I}^{nc}} \tag{12}$$

Further, from Equation (10) it follows that $\tau_{dissI}/\tau_{diss0} = K_{340}^{c}/K_{34I}^{c}$ (see SI, Eq. S32, for details) and then from Equations (9) and (12) that:

$$\frac{K_{340}^{c}}{K_{34I}^{c}} \approx \frac{K_{340}^{nc}}{K_{34I}^{nc}} \cdot \frac{k_{4I}^{nc}}{k_{40}^{nc}}, \tag{13}$$

Here the left hand side corresponds to $\tau_{dissI}/\tau_{diss0}$ and the right hand side to d_{e0}^{nc}/d_{eI}^{nc} in Equation (9). Accordingly, the d_{eI}^{nc} reduction may be due to a decrease in the equilibrium constant K_{34I}^{nc}, an increase in the rate constant, k_{4I}^{nc} or a combination thereof.

In the previous section we concluded that $k_{4I}^{c} = k_{40}^{c}$, but what about the near-cognate GTPase rate constants appearing in Equation (13)? An answer to this question is provided by crystallographic data showing virtually no structural changes of the decoding center or the geometry of the codon-anticodon helix in state C_4 in response to aminoglycoside addition in near-cognate cases (51,56). Following the same logic as in the previous section we propose from these structural data that aminoglycosides leave not only cognate but also near-cognate GTPase rate constants unaltered ($k_{4I}^{nc} \approx k_{40}^{nc}$). Then, it follows from Equation (13) that aminoglycosides reduce equilibrium constants K_{340}^{nc} and K_{340}^{c} by the very same factor. The d_{e0}^{nc} -value reductions are then completely explained by the aminoglycoside-induced reductions in K_{340}^{nc} at unaffected k_{40}^{nc}.

The premise $k_{4I}^{nc} \approx k_{40}^{nc}$ leads, however, to an apparent problem: if aminoglycosides only affect K_{340}^{nc} and K_{340}^{c} how then can paromomycin increase the Michaelis-Menten constant, k_{cat0}^{nc}, of the near-cognate GTP hydrolysis reaction from about 6 s^{-1} to about 80 s^{-1} (see Supplementary Figure S4)? To explain this result we first note that k_{catI}^{x} for the scheme in Figure 5 is given by (see SI, Eq. S8, for details):

$$k_{catI}^{x} = 1/\left[\frac{1}{k_2}(1 + a_{3I}^{x}(1 + a_{4I}^{x})) + \frac{1}{k_{3I}}(1 + a_{4I}^{x}) + \frac{1}{k_{4I}^{x}}\right] \tag{14}$$

In cognate cases the discard parameters a_{30}^{c} and a_{40}^{c} are much smaller than one and decrease further upon aminoglycoside addition, so that:

$$k_{catI}^{c} \approx 1/\left[\frac{1}{k_2} + \frac{1}{k_{3I}} + \frac{1}{k_{40}^{c}}\right], \tag{15}$$

where we used that $k_{4I}^{c} = k_{40}^{c}$ (see above in Discussion). This suggests that the cognate k_{catI}^{c} will display but a moderate increase in response to aminoglycoside addition due to increased k_{3I}-value. In near-cognate cases, in contrast, the discard parameters a_{30}^{nc} and a_{40}^{nc} are much larger than one but become greatly reduced by aminoglycosides. These features explain (see Equation 14) why k_{cat0}^{nc} is so much smaller than k_{cat0}^{c} and why aminoglycosides greatly increase k_{cat0}^{nc} at unaltered $k_{4I}^{nc} \approx k_{40}^{nc}$. It also follows (see SI, Eq. S10, for details) that when $k_{4I}^{nc} \approx k_{40}^{nc}$ the increase in k_{cat0}^{nc} by aminoglycosides is near proportional to the aminoglycoside-induced decrease in d_{e0}^{nc}. Indeed, the 14-fold increase in k_{cat0}^{nc} by paromomycin (from 6 s^{-1} to about 80 s^{-1}) is close to the 16 fold decrease in d_{e0}^{nc} by this drug (Table 2).

Above we concluded that the reduction in d_{eI}^{nc} by aminoglycosides is caused by a reduction in K_{34I}^{nc} (see Equation 12). It follows from Equations (6) and (7) that d_{eI}^{nc} can also be written as:

$$d_{eI}^{nc} \approx a_{3I}^{nc} a_{4I}^{nc} = D_I^{nc}(a_{3I}^{c} a_{4I}^{c}) = D_I^{nc} a_I^{c} \tag{16}$$

Equation (16) implies that any reduction in d_{eI}^{nc} at unaltered D_I^{nc} must be mirrored by a corresponding reduction in the combined discard parameter $a_I^{c} = a_{3I}^{c} a_{4I}^{c}$ for cognate codon reading. At 2.3 mM free [Mg^{2+}], at which the dissociation times, τ_{dissI}, for GTPase deficient cognate T_3 were measured (Table 1) the discard parameter $a_2 \approx 1$ (28). Also taking into account that $\tau_{diss0} \approx 2$ s (Table 1) and $k_{40}^{c} > 900$ s^{-1} (44) Equation (10) can be used to estimate an upper bound for a_0^{c} as 10^{-3}. This means that the fraction of the intrinsic selectivity that is expressed in the effective selectivity is smaller than 1 per mille and that aminoglycosides reduce this remarkably small fraction even further. We note that these extremely small values of a_0^{c} and a_I^{c} can be traced to the near irreversibility of the cognate reaction upon formation of codon-anticodon contact in state C_3. With $a_0^{c} = 10^{-3}$ and $d_{e0}^{UCC} = 5700$ (Table 1) and use of Equation (16) we estimate $D_0^{UCC} \approx d_{e0}^{UCC}/a_0^{c}$ as $5.7 \cdot 10^6$. This value is surprisingly high and, yet, in good agreement with the value $D_0^{UCC} = 2.7 \times 10^6$ calculated from the rate constants of initial selection, as reported by Rodnina and collaborators (7) and also with the value of D_0^{UCC} in the range $0.6 \times 10^6 - 3.4 \times 10^6$, as estimated from molecular dynamic simulations by Åqvist *et al.* (61) for T_3 with Phe-$tRNA^{Phe}$ reading its near-cognate UCC codon.

Past results in the context of the present study

Ramakrishnan and co-workers measured the effect of paromomycin (Par) on the affinity of anticodon stem-loop (ASL) constructs to 70S ribosomes programmed with short mRNA analogues (14). They found that Par increased the ribosome affinity to a cognate ASL about 15-fold (14), similar to the Par induced increase in dissociation time of a GTPase-deficient cognate T_3 from the 70S ribosome observed here (Table 2). They also found that the effect of Par on near-cognate ASLs was insignificant (14). Also the latter result is perfectly in line with the present data, provided that the equilibrium constant K_{34I}^{nc} remained considerably larger than one after a 15-fold decrease in response to Par addition (see SI, Eq. S40, for details).

Rodnina and collaborators used fast kinetics and T_3s with fluorescence labeled tRNA to study the effects of Par on codon reading (30). These studies were conducted with a low fidelity (LoFi) buffer (7), which lacked the polyamines required for cell-free protein synthesis of physiological relevance (23,24,27,63–65). Since there was virtually no initial codon selection either with or without Par (i.e. $A_P^{nc} \approx A_0^{nc} \approx 1$), the effects of Par on the elemental rate constants they observed (30) could not be related to the Par-induced decrease

in the accuracy of initial selection that occurs under physiological conditions. Namely, under conditions where the accuracy of our *in vitro* translation matches that *in vivo* (28), Par decreased the accuracy of initial selection on the UCC codon by a Phe-tRNA^{Phe} containing T_3 from $A_0^{UCC} \approx 2900$ down to $A_P^{UCC} \approx 200$ (Figure 3B). We also note that while we used a four state scheme to describe initial codon selection (Figure 5), Rodnina and collaborators used a three-state scheme (Equation 17) to describe the same process. In essence, this amounts to a contraction of our states C_3 and C_4 in Figure 5 to a single state C_{34}, in which the distinction between active and inactive monitoring bases is blurred:

$$R_1 + T_3 \underset{q_2}{\overset{k_1}{\rightleftharpoons}} C_2 \underset{q^x_{e3I}}{\overset{k_2}{\rightleftharpoons}} C_{34} \xrightarrow{k^x_{e3I}} \qquad (17)$$

Rodnina *et al.* concluded that Par decreased k_2 in both cognate and near-cognate cases about trice (30). It can also be calculated from their elemental rate constants (Table 2 in (30)) that because of this k_2 reduction the Michaelis-Menten constant k_{cat} of the near-cognate GTP hydrolysis reaction was increased by Par only slightly, from 30 s^{-1} to 34 s^{-1}. From the present data follows that k_2 was insensitive to aminoglycosides, and that Par induced an increase in the near-cognate k_{cat}-value for GTP-hydrolysis from 6 to 80 s^{-1} (Supplementary Figure S4). One explanation for these discrepancies could be their low temperature (20°C) and polyamine deficient conditions compared to our high temperature (37°C) and polyamine proficient conditions. Another explanation could be the approximate nature of the elemental rate constant estimations from their fluorescence based data (see Supplementary Discussion for details).

Rodnina and collaborators also concluded that Par decreased the near-cognate dissociation rate constant q^{nc}_{e30} (their k_{-2}) in Equation (17) from 17 to 3.5 s^{-1} and increased the near-cognate GTPase rate constant k^{nc}_{e30} (their k_3) from 50 to about 500 s^{-1} at unchanged cognate GTPase rate constant k^{c}_{e30} (about 500 s^{-1}) (30). Concerning Par-induced changes in these parameters, we first note that q^{nc}_{e3I} and k^{nc}_{e3I} in Equation (17) are related to the elemental rate and equilibrium constants of the scheme in Figure 5 as $q^{nc}_{e3I} = q^{nc}_3 K^{nc}_{34I}/(K^{nc}_{34I} + 1)$ and $k^{nc}_{e3I} = k^{nc}_{4I}/(K^{nc}_{34I} + 1)$, respectively (see SI, Eq. S44, for details). A large reduction in K^{nc}_{340} by Par leads, therefore, directly to a large decrease in q^{nc}_{e30} and a large increase in k^{nc}_{e30} even at unaltered near-cognate GTPase rate constant $k^{nc}_{4I} = k^{nc}_{40}$. It is, we propose, the contraction of the four-state kinetic scheme in Figure 5 to the three-state scheme in Equation (17) that is the main reason for the apparent discrepancy between the present conclusion that Par has no effect on k^{nc}_{40} and only decreases equilibrium constant K^{nc}_{340} for monitoring bases activation and the previous conclusion that Par increases the near-cognate GTPase rate constant by an order of magnitude (30,32).

The role of induced fit in initial codon selection

The notion of induced fit generally refers to reorganization of the catalytic center of an enzyme in response to substrate binding (38,39). The present four-state scheme (Figure 5) describes an induced fit mechanism of initial codon selection in which the binding of cognate and near-cognate T_3s lead to similar reorganizations of the ribosome decoding center. In this respect the present mechanism differs significantly from previously suggested induced fit mechanisms of initial codon selection, as explained below.

We first note that in the absence of drugs the compounded GTPase rate constant k^x_{e30} in the contracted scheme of Equation (17) is approximated by $k^x_{e30} = k^x_{40}/(K^x_{340} + 1)$ (see SI, Eq. S44, for details). Accordingly, even in the case when $k^{nc}_{40} \approx k^c_{40}$, the comparatively small values observed for k^{nc}_{e30} (7,24,41) are easily explained by comparatively large values of $K^{nc}_{340} >> K^c_{340}$. Those reflect a comparatively large standard free energy cost for binding of the monitoring bases A1492, A1493 and G530 to a near-cognate compared to a cognate codon-anticodon helix and concomitant 'closure' of the 30S subunit (14). In contrast, Rodnina and collaborators explained small k^{nc}_{e30} values by suggesting that GTP hydrolysis in near-cognate cases occurs in the 'open' state of the 30S subunit with inactive monitoring bases, i.e. in a state corresponding to C_3 in Figure 5 (24,40). This 'induced fit' mechanism favors cognate in relation to near-cognate T_3s (38) by allowing only cognate T_3s to reach state C_4 and from there proceed to GTP hydrolysis via an optimal transition state. Near-cognate T_3s, in contrast, are only able to reach state C_3, from which they proceed to a suboptimal transition state for GTP hydrolysis (1,14,24,40). It has also been suggested that aminoglycosides greatly reduce the standard free energy cost to reach state C_4 from state C_3 thereby redirecting near-cognate T_3s to follow the pathway of cognate T_3s to rapid GTP hydrolysis via state C_4 (1,66). This particular induced fit mechanism was challenged by crystal structures of the mRNA programmed ribosome with near-cognate, deacylated tRNAs in their A sites (51,56,67–70) and more recently by cryo-EM structures of near-cognate ternary complexes bound to mRNA programmed ribosomes (46). These structures demonstrate that even in the absence of drugs near-cognate T_3 can reach state C_4 in Figure 5 with a near-cognate codon-anticodon helix in authentic contact with the monitoring bases and the 30S subunit closed around the ASL of the tRNA. The implication here is that cognate and near-cognate T_3 can proceed to GTP hydrolysis via structurally very similar ground states in C_4 and, hence, have very similar transition state free energy barriers for GTP hydrolysis (i.e. $\Delta G^{nc}_{4,\#} = \Delta G^{c}_{4,\#}$). In this new picture, similar to that suggested by Åqvist and collaborators (61), $k^{nc}_{40} \approx k^c_{40}$ but the standard free energy cost to reach the pre-GTP hydrolysis state C_4 is much higher for near-cognate than cognate T_3. Moreover, when $k^{nc}_{40} \approx k^c_{40}$, it follows from Equation (8) that $\Delta G^{nc}_{1,\#} - \Delta G^{c}_{1,\#} = \Delta G^{nc}_{2,4I} - \Delta G^{c}_{2,4I}$(see SI, Eq. S21 for details). Since in state C_2 cognate and near-cognate T_3s have the same standard free energy, it also follows that the intrinsic selectivity D^{nc}_I is solely determined by the difference in standard free energy between near-cognate and cognate T_3s in state C_4. Thus, induced fit *per se* does not conjure increased intrinsic selectivity D^{nc}_I (39).

Now, if the intrinsic, ultimate, selectivity, D^{nc}_I, is unaffected by induced fit, what about the effective selectivity, d^{nc}_{eI}? To answer this question we recast Equation (12) for d^{nc}_{eI}

(see SI, Eq. S16, for details) in the form:

$$d_{eI}^{nc} \approx K_{23}^{nc} K_{34I}^{nc} \frac{k_2}{k_{4I}^{nc}} = \frac{k_2}{k_{4I}^{nc}} \cdot \exp(\Delta G_{2,4I}^{nc}/RT) \qquad (18)$$

It is seen that at a constant k_2/k_{4I}^{nc} ratio, the effective selectivity d_{eI}^{nc} increases with increasing $\Delta G_{2,4I}^{nc}$ gap size. We further note that in state C_2 of the present induced fit model (Figure 5) there is no codon-anticodon contact, monitoring bases are inactive and the 30S subunit is in the open form. It is only in state C_4 the three conditions for GTP hydrolysis are fulfilled, i.e. codon-anticodon contact is established, monitoring bases are all active and the 30S subunit closed. This implies that the near-cognate standard free energy cost, $\Delta G_{2,4I}^{nc}$, to move from state C_2 to state C_4 is comparatively large (2,14), and, hence, according to Equation (18), d_{eI}^{nc}-value is also comparatively large. In contrast, in a hypothetical situation without induced fit, the monitoring bases could be activated and the 30S subunit closed already in state C_2 in the absence of the codon-anticodon contact. Accordingly, without the induced fit, the near-cognate standard free energy gap $\Delta G_{2,4I}^{nc}$ from state C_2 to C_4 would be smaller, the d_{eI}^{nc}-value also smaller and the frequency of initial codon selection errors would be larger. In general, the more similar the structures of the decoding center in states C_2 and C_4, the smaller the free energy gap, $\Delta G_{2,4I}^{nc}$, and the smaller the d_{eI}^{nc}-value, the error induction by aminoglycosides described here being a special case of this general principle.

Another inference from the statement that $\Delta G_{2,4I}^{nc}$ is the main determinant of the effective selectivity, d_{eI}^{nc} (Equation 18) is that the existence of an intermediate state C_3, with codon-anticodon contact in an aqueous environment (Figure 5), or of other putative states between C_2 and C_4, will not affect the d_{eI}^{nc}-value. It follows, therefore, that the induced fit mechanism without state C_3 proposed by Yusupov/Yusupova and collaborators (51,67) has the same effective selectivity d_{eI}^{nc} as the mechanism in Figure 5, provided that the k_2/k_{4I}^{nc} ratio and $\Delta G_{2,4I}^{nc}$ are the same. In their mechanism the rearrangement of the decoding center proceeds directly from state C_2 to C_4 as the A-site tRNA bends and its ASL enters the decoding center. In particular, they suggested that the entering ASL disrupts the stacking between A1492 and A1913, thereby activating A1492 to interact with the second position of the codon-anticodon helix (51,67). Subsequently, interaction between G530 and activated A1492 induces ribosome closure for both cognate and near-cognate T_3s alike, so that the codon-anticodon contact occurs in the water-free environment of state C_4 (67). In cognate cases this contact is stable and complex C_4 rapidly moves forward to GTP hydrolysis. In near-cognate cases this contact is unstable and complex C_4 rapidly moves backward to complex C_2 (51,67). However attractive, this 'direct induced fit' mechanism seems to be at odds with a recent cryo-EM study, in which state C_3 was directly observed (46). It is tempting to speculate that the intermediate state C_3 confers a kinetic advantage to the mechanism in Figure 5 by providing an indirect but faster route from C_2 to C_4 that avoids a predictably difficult 'one step' water expulsion from the 'tight and rigid' decoding center (51) by the incoming ASL of tRNA (14).

In summary, we suggest that initial codon selection benefits from an induced fit mechanism which increases the effective selectivity, current accuracy and speed of codon reading at unaltered intrinsic selectivity of the ribosome. By this mechanism (Figure 5), aminoglycosides reduce the effective selectivity and the current accuracy of initial codon selection by an equal reduction of the standard free energy cost for ribosome movement from state C_2 to state C_4 in cognate and near-cognate cases.

SUPPLEMENTARY DATA

Supplementary Data are available at NAR Online.

ACKNOWLEDGEMENTS

We thank Drs Joseph Puglisi and Magnus Johansson for critical reading of the manuscript. We are grateful to Dr Suparna Sanyal for providing us with purified H84A EF-Tu mutant protein.

FUNDING

Knut and Alice Wallenberg foundation (RiboCORE); Swedish Research Council and the Human Frontier Science Program (to M.E.). Funding for open access charge: Knut and Alice Wallenberg foundation (RiboCORE); Swedish Research Council and the Human Frontier Science Program (to M.E.).
Conflict of interest statement. None declared.

REFERENCES

1. Ogle,J.M., Carter,A.P. and Ramakrishnan,V. (2003) Insights into the decoding mechanism from recent ribosome structures. *Trends Biochem. Sci.*, **28**, 259–266.
2. Ogle,J.M. and Ramakrishnan,V. (2005) Structural insights into translational fidelity. *Annu. Rev. Biochem.*, **74**, 129–177.
3. Schmeing,T.M. and Ramakrishnan,V. (2009) What recent ribosome structures have revealed about the mechanism of translation. *Nature*, **461**, 1234–1242.
4. Voorhees,R.M. and Ramakrishnan,V. (2013) Structural basis of the translational elongation cycle. *Annu. Rev. Biochem.*, **82**, 203–236.
5. Reuveni,S., Ehrenberg,M. and Paulsson,J. (2017) Ribosomes are optimized for autocatalytic production. *Nature*, **547**, 293–297.
6. Ehrenberg,M. and Kurland,C.G. (1984) Costs of accuracy determined by a maximal growth rate constraint. *Q. Rev. Biophys.*, **17**, 45–82.
7. Gromadski,K.B., Daviter,T. and Rodnina,M.V. (2006) A uniform response to mismatches in codon-anticodon complexes ensures ribosomal fidelity. *Mol. Cell*, **21**, 369–377.
8. Johansson,M., Lovmar,M. and Ehrenberg,M. (2008) Rate and accuracy of bacterial protein synthesis revisited. *Curr. Opin. Microbiol.*, **11**, 141–147.
9. Zhang,J., Ieong,K.W., Johansson,M. and Ehrenberg,M. (2015) Accuracy of initial codon selection by aminoacyl-tRNAs on the mRNA-programmed bacterial ribosome. *Proc. Natl. Acad. Sci. U.S.A.*, **112**, 9602–9607.
10. Ieong,K.W., Uzun,U., Selmer,M. and Ehrenberg,M. (2016) Two proofreading steps amplify the accuracy of genetic code translation. *Proc. Natl. Acad. Sci. U.S.A.*, **113**, 13744–13749.
11. Borg,A. and Ehrenberg,M. (2015) Determinants of the rate of mRNA translocation in bacterial protein synthesis. *J. Mol. Biol.*, **427**, 1835–1847.
12. Johansson,M., Zhang,J. and Ehrenberg,M. (2012) Genetic code translation displays a linear trade-off between efficiency and accuracy of tRNA selection. *Proc. Natl. Acad. Sci. U.S.A.*, **109**, 131–136.

13. Ogle,J.M., Brodersen,D.E., Clemons,W.M. Jr, Tarry,M.J., Carter,A.P. and Ramakrishnan,V. (2001) Recognition of cognate transfer RNA by the 30S ribosomal subunit. *Science*, **292**, 897–902.
14. Ogle,J.M., Murphy,F.V., Tarry,M.J. and Ramakrishnan,V. (2002) Selection of tRNA by the ribosome requires a transition from an open to a closed form. *Cell*, **111**, 721–732.
15. Hopfield,J.J. (1974) Kinetic proofreading: a new mechanism for reducing errors in biosynthetic processes requiring high specificity. *Proc. Natl. Acad. Sci. U.S.A.*, **71**, 4135–4139.
16. Ninio,J. (1975) Kinetic amplification of enzyme discrimination. *Biochimie*, **57**, 587–595.
17. Ehrenberg,M. and Blomberg,C. (1980) Thermodynamic constraints on kinetic proofreading in biosynthetic pathways. *Biophys. J.*, **31**, 333–358.
18. Freter,R.R. and Savageau,M.A. (1980) Proofreading systems of multiple stages for improved accuracy of biological discrimination. *J. Theor. Biol.*, **85**, 99–123.
19. Thompson,R.C. and Stone,P.J. (1977) Proofreading of the codon-anticodon interaction on ribosomes. *Proc. Natl. Acad. Sci. U.S.A.*, **74**, 198–202.
20. Ruusala,T., Ehrenberg,M. and Kurland,C.G. (1982) Is there proofreading during polypeptide synthesis? *EMBO J.*, **1**, 741–745.
21. Kramer,E.B. and Farabaugh,P.J. (2007) The frequency of translational misreading errors in E. coli is largely determined by tRNA competition. *RNA*, **13**, 87–96.
22. Manickam,N., Nag,N., Abbasi,A., Patel,K. and Farabaugh,P.J. (2014) Studies of translational misreading in vivo show that the ribosome very efficiently discriminates against most potential errors. *RNA*, **20**, 9–15.
23. Jelenc,P.C. and Kurland,C.G. (1979) Nucleoside triphosphate regeneration decreases the frequency of translation errors. *Proc. Natl. Acad. Sci. U.S.A.*, **76**, 3174–3178.
24. Gromadski,K.B. and Rodnina,M.V. (2004) Kinetic determinants of high-fidelity tRNA discrimination on the ribosome. *Mol. Cell*, **13**, 191–200.
25. Wohlgemuth,I., Pohl,C., Mittelstaet,J., Konevega,A.L. and Rodnina,M.V. (2011) Evolutionary optimization of speed and accuracy of decoding on the ribosome. *Philos. Trans. R Soc. Lond. B Biol. Sci.*, **366**, 2979–2986.
26. Studer,S.M., Feinberg,J.S. and Joseph,S. (2003) Rapid kinetic analysis of EF-G-dependent mRNA translocation in the ribosome. *J. Mol. Biol.*, **327**, 369–381.
27. Nierhaus,K.H. (2014) Mg2+, K+, and the ribosome. *J. Bacteriol.*, **196**, 3817–3819.
28. Zhang,J., Ieong,K.W., Mellenius,H. and Ehrenberg,M. (2016) Proofreading neutralizes potential error hotspots in genetic code translation by transfer RNAs. *RNA*, **22**, 896–904.
29. Alatossava,T., Jutte,H., Kuhn,A. and Kellenberger,E. (1985) Manipulation of intracellular magnesium content in polymyxin B nonapeptide-sensitized Escherichia coli by ionophore A23187. *J. Bacteriol.*, **162**, 413–419.
30. Pape,T., Wintermeyer,W. and Rodnina,M.V. (2000) Conformational switch in the decoding region of 16S rRNA during aminoacyl-tRNA selection on the ribosome. *Nat. Struct. Biol.*, **7**, 104–107.
31. Rodnina,M.V. and Wintermeyer,W. (2001) Fidelity of aminoacyl-tRNA selection on the ribosome: kinetic and structural mechanisms. *Annu. Rev. Biochem.*, **70**, 415–435.
32. Gromadski,K.B. and Rodnina,M.V. (2004) Streptomycin interferes with conformational coupling between codon recognition and GTPase activation on the ribosome. *Nat. Struct. Mol. Biol.*, **11**, 316–322.
33. Cabanas,M.J., Vazquez,D. and Modolell,J. (1978) Inhibition of ribosomal translocation by aminoglycoside antibiotics. *Biochem. Biophys. Res. Commun.*, **83**, 991–997.
34. Tsai,A., Uemura,S., Johansson,M., Puglisi,E.V., Marshall,R.A., Aitken,C.E., Korlach,J., Ehrenberg,M. and Puglisi,J.D. (2013) The impact of aminoglycosides on the dynamics of translation elongation. *Cell Rep.*, **3**, 497–508.
35. Fourmy,D., Recht,M.I., Blanchard,S.C. and Puglisi,J.D. (1996) Structure of the A site of Escherichia coli 16S ribosomal RNA complexed with an aminoglycoside antibiotic. *Science*, **274**, 1367–1371.
36. Recht,M.I., Fourmy,D., Blanchard,S.C., Dahlquist,K.D. and Puglisi,J.D. (1996) RNA sequence determinants for aminoglycoside binding to an A-site rRNA model oligonucleotide. *J. Mol. Biol.*, **262**, 421–436.
37. Carter,A.P., Clemons,W.M., Brodersen,D.E., Morgan-Warren,R.J., Wimberly,B.T. and Ramakrishnan,V. (2000) Functional insights from the structure of the 30S ribosomal subunit and its interactions with antibiotics. *Nature*, **407**, 340–348.
38. Koshland,D.E. (1958) Application of a theory of enzyme specificity to protein synthesis. *Proc. Natl. Acad. Sci. U.S.A.*, **44**, 98–104.
39. Fersht,A. (1977) *Enzyme Structure and Mechanism*. 1977 edn. W.H. Freeman and Company, NY.
40. Daviter,T., Gromadski,K.B. and Rodnina,M.V. (2006) The ribosome's response to codon-anticodon mismatches. *Biochimie*, **88**, 1001–1011.
41. Pape,T., Wintermeyer,W. and Rodnina,M.V. (1998) Complete kinetic mechanism of elongation factor Tu-dependent binding of aminoacyl-tRNA to the A site of the E. coli ribosome. *EMBO J.*, **17**, 7490–7497.
42. Daviter,T., Wieden,H.J. and Rodnina,M.V. (2003) Essential role of histidine 84 in elongation factor Tu for the chemical step of GTP hydrolysis on the ribosome. *J. Mol. Biol.*, **332**, 689–699.
43. Wold,F. and Ballou,C.E. (1957) Studies on the enzyme enolase. I. Equilibrium studies. *J Biol Chem*, **227**, 301–312.
44. Johansson,M., Bouakaz,E., Lovmar,M. and Ehrenberg,M. (2008) The kinetics of ribosomal peptidyl transfer revisited. *Mol. Cell*, **30**, 589–598.
45. Borovinskaya,M.A., Pai,R.D., Zhang,W., Schuwirth,B.S., Holton,J.M., Hirokawa,G., Kaji,H., Kaji,A. and Cate,J.H. (2007) Structural basis for aminoglycoside inhibition of bacterial ribosome recycling. *Nat Struct Mol Biol*, **14**, 727–732.
46. Loveland,A.B., Demo,G., Grigorieff,N. and Korostelev,A.A. (2017) Ensemble cryo-EM elucidates the mechanism of translation fidelity. *Nature*, **546**, 113–117.
47. Blanchard,S.C., Gonzalez,R.L., Kim,H.D., Chu,S. and Puglisi,J.D. (2004) tRNA selection and kinetic proofreading in translation. *Nat. Struct. Mol. Biol.*, **11**, 1008–1014.
48. Pavlov,M.Y., Liljas,A. and Ehrenberg,M. (2017) A recent intermezzo at the ribosome club. *Philos. Trans. R. Soc. Lond. B Biol. Sci.*, **372**, 20160185.
49. Nissen,P., Kjeldgaard,M., Thirup,S., Polekhina,G., Reshetnikova,L., Clark,B.F. and Nyborg,J. (1995) Crystal structure of the ternary complex of Phe-tRNAPhe, EF-Tu, and a GTP analog. *Science*, **270**, 1464–1472.
50. Pape,T., Wintermeyer,W. and Rodnina,M. (1999) Induced fit in initial selection and proofreading of aminoacyl-tRNA on the ribosome. *EMBO J.*, **18**, 3800–3807.
51. Demeshkina,N., Jenner,L., Westhof,E., Yusupov,M. and Yusupova,G. (2013) New structural insights into the decoding mechanism: translation infidelity via a G.U pair with Watson-Crick geometry. *FEBS Lett.*, **587**, 1848–1857.
52. Valle,M., Sengupta,J., Swami,N.K., Grassucci,R.A., Burkhardt,N., Nierhaus,K.H., Agrawal,R.K. and Frank,J. (2002) Cryo-EM reveals an active role for aminoacyl-tRNA in the accommodation process. *EMBO J.*, **21**, 3557–3567.
53. Stark,H., Rodnina,M.V., Wieden,H.J., Zemlin,F., Wintermeyer,W. and van Heel,M. (2002) Ribosome interactions of aminoacyl-tRNA and elongation factor Tu in the codon-recognition complex. *Nat. Struct. Biol.*, **9**, 849–854.
54. Schmeing,T.M., Voorhees,R.M., Kelley,A.C., Gao,Y.G., Murphy,F.V.t., Weir,J.R. and Ramakrishnan,V. (2009) The crystal structure of the ribosome bound to EF-Tu and aminoacyl-tRNA. *Science*, **326**, 688–694.
55. Selmer,M., Dunham,C.M., Murphy,F.V.t., Weixlbaumer,A., Petry,S., Kelley,A.C., Weir,J.R. and Ramakrishnan,V. (2006) Structure of the 70S ribosome complexed with mRNA and tRNA. *Science*, **313**, 1935–1942.
56. Demeshkina,N., Jenner,L., Westhof,E., Yusupov,M. and Yusupova,G. (2012) A new understanding of the decoding principle on the ribosome. *Nature*, **484**, 256–259.
57. Fischer,N., Neumann,P., Konevega,A.L., Bock,L.V., Ficner,R., Rodnina,M.V. and Stark,H. (2015) Structure of the E. coli ribosome-EF-Tu complex at <3 A resolution by Cs-corrected cryo-EM. *Nature*, **520**, 567–570.

58. Rodnina,M.V., Fricke,R., Kuhn,L. and Wintermeyer,W. (1995) Codon-dependent conformational change of elongation factor Tu preceding GTP hydrolysis on the ribosome. *EMBO J.*, **14**, 2613–2619.
59. Panecka,J., Mura,C. and Trylska,J. (2014) Interplay of the bacterial ribosomal A-site, S12 protein mutations and paromomycin binding: a molecular dynamics study. *PLoS One*, **9**, e111811.
60. Rodnina,M.V., Pape,T., Fricke,R., Kuhn,L. and Wintermeyer,W. (1996) Initial binding of the elongation factor Tu.GTP.aminoacyl-tRNA complex preceding codon recognition on the ribosome. *J. Biol. Chem.*, **271**, 646–652.
61. Satpati,P., Sund,J. and Aqvist,J. (2014) Structure-based energetics of mRNA decoding on the ribosome. *Biochemistry*, **53**, 1714–1722.
62. Schuette,J.C., Murphy,F.V.t., Kelley,A.C., Weir,J.R., Giesebrecht,J., Connell,S.R., Loerke,J., Mielke,T., Zhang,W., Penczek,P.A. *et al.* (2009) GTPase activation of elongation factor EF-Tu by the ribosome during decoding. *EMBO J.*, **28**, 755–765.
63. Ehrenberg,M. and Kurland,C.G. (1988) Measurement of translational kinetic parameters. *Methods Enzymol.*, **164**, 611–631.
64. Bartetzko,A. and Nierhaus,K.H. (1988) Mg2+/NH4+/polyamine system for polyuridine-dependent polyphenylalanine synthesis with near in vivo characteristics. *Methods Enzymol.*, **164**, 650–658.
65. Igarashi,K. and Kashiwagi,K. (2010) Modulation of cellular function by polyamines. *Int. J. Biochem. Cell Biol.*, **42**, 39–51.
66. Rodnina,M.V. and Wintermeyer,W. (2001) Ribosome fidelity: tRNA discrimination, proofreading and induced fit. *Trends Biochem. Sci.*, **26**, 124–130.
67. Rozov,A., Demeshkina,N., Westhof,E., Yusupov,M. and Yusupova,G. (2015) Structural insights into the translational infidelity mechanism. *Nat. Commun.*, **6**, 7251.
68. Rozov,A., Demeshkina,N., Westhof,E., Yusupov,M. and Yusupova,G. (2016) New structural insights into translational miscoding. *Trends Biochem. Sci.*, **41**, 798–814.
69. Rozov,A., Westhof,E., Yusupov,M. and Yusupova,G. (2016) The ribosome prohibits the G*U wobble geometry at the first position of the codon-anticodon helix. *Nucleic Acids Res.*, **44**, 6434–6441.
70. Rozov,A., Demeshkina,N., Khusainov,I., Westhof,E., Yusupov,M. and Yusupova,G. (2016) Novel base-pairing interactions at the tRNA wobble position crucial for accurate reading of the genetic code. *Nat. Commun.*, **7**, 10457.